Dynamics of Crack Propagation in Brittle Materials

J. Boudet, S. Ciliberto, V. Steinberg

J. Phys. II France 6 (1996) 1493–1516 OCTOBER 1996, PAGE 1493

Dynamics of Crack Propagation in Brittle Materials

J.F. Boudet, S. Ciliberto (*) and V. Steinberg (**)

Laboratoire de Physique (***), École Normale Supérieure de Lyon, 46 allée d'Italie, 69364 Lyon Cedex 07, France

(Received 13 October 1995, revised 6 May 1996, accepted 2 July 1996)

PACS.47.30.Nz – Fracture mechanics, fatigue, and craks
PACS.62.20.Mk – Fatigue, brittleness, fracture, and crack

Abstract. — An experimental study of the properties of crack propagation in brittle materials is described. Specifically the crack speed, the sound emission and the fracture profile have been measured as a function of the applied stress. We find that the local velocity can be considered as a control parameter which determines the properties of the crack. The steady state velocity turns out to be a function of the applied stress. Several thresholds have been identified. One corresponds to the presence of a weak sound emission associated with velocity oscillations and another one to the onset of the surface roughness associated with a strong sound emission. We also find a strong crosscorrelation between sound and velocity oscillations. The statistical properties of the fracture profile depend on the steady state velocity.

1. Introduction

The dynamics of crack propagation in brittle materials is an interesting non-linear pattern forming phenomenon, which bears several analogies with other interface problems, such as, for example, directional solidification and crystal growth. In these two phenomena the interface can be smooth or rough depending on the speed of the front propagation and on the growth rate, respectively. Similarly the surface of a fracture can be smooth or rough depending on the velocity of crack propagation. At very high velocity the well known phenomenon of crack branching may appear [1]. High resolution velocity measurements [3, 6, 7] of a crack propagation reveal the existence of a critical velocity V_c above which the dynamics of the crack change drastically: the velocity of the crack exhibits strong oscillations and the roughness of the crack surface grows significantly. Subsequent experimental [4–7], numerical [8, 9], and analytical [10–16] results shed light on various aspects of the phenomenon under consideration.

One of the key questions of the fracture dynamics is what selects the crack propagation velocity and what mechanism limits it. A commonly accepted view is that the crack speed is limited only by the rate at which a stored elastic energy is transferred to the crack tip. It leads immediately to the conclusion that the Rayleigh sound velocity V_R along a free fracture surface is considered to be the limiting crack speed [1]. However, it has been known for a

(*) Author for correspondence (e-mail: ciliberto@physique.ens-lyon.fr)
(**) on leave from, Department of Physics of Complex Systems, The Weizmann Institute of Science, Rehovot 76100, Israel.
(***) URA 1325 C.N.R.S.

while [1] and particularly, verified quantitatively in the recent experiments [3–7] that at least in the brittle amorphous materials the maximum crack speed approaches just a fraction of V_R. One of the reasons for this discrepancy is the occurrence of the dynamic instability, mentioned above, which is related to the onset of new and more effective ways of energy dissipation. This instability might be associated with the formation of microcracks, on the side of the main crack, which increases the energy dissipation by increasing the fracture surface [7]. Furthermore at higher velocities the well known phenomenon of macrobranching takes place. Thus, it looks like micro- and macrobranching is a common way for Nature to effectively increase the energy dissipation. However if the crack maximum propagation speed is certainly limited by the rate of energy dissipation, the possibility of having a domain of limiting velocities [6, 7] still remains an open problem, which could not be uniquely linked with the above mentioned mechanisms. Indeed the limiting velocity of the crack seems to be determined by the amount of the elastic energy stored into the sample [6,7,9,11]. Thus it is very important to investigate the relationship between energy transfer and energy dissipation rate.

Another important issue, in the study of crack dynamics, is, *e.g.*, how different physical parameters which can be measured during fracture such as the stress, necessary to brake the material, the steady state velocity of the crack, the level of sound emitted, the heating of the crack tip and the profile of the crack surfaces, are linked together. There are many attempts to explain, for example the interaction of sound wave with the crack instability. A very recent one is the theory proposed by Lund [16], which considers a force acting transversely on the crack tip, which is the analogue of the Lorentz force in electrodynamics. This force, of course, does not produce any work and therefore cannot be taken into account by simple energy considerations [1]. In any case the onset of this instability, and the influence of ultrasound waves on the crack propagation, still remain an open problem.

In this paper we extend previous experimental studies of references [3, 4, 7] and we focus on the relationship which may exist among different quantities, such as the crack propagation speed, the sound emission, the surface roughness and the applied stress during fracture. First we show that the steady state velocity of the crack can be varied by preparing (in samples of equal width) an initial crack in different ways [6]. This allows us to establish a relationship between the steady state velocity V_f reached by the crack and the actual stress applied to the sample at the beginning of the crack motion. This is an interesting result because the asymptotic speed was considered previously to have just one possible value which is a fraction of V_R. Second, we will show that the local velocity $V(t)$ determines many properties of the crack such as the surface roughness, its statistical properties and the amplitude of sound emitted. Specifically when $V(t) < V_c$ the crack surfaces are smooth whereas when $V(t) > V_c$ the surfaces produced by the crack are rough and a strong sound emission occurs. Finally we have characterized the statistical properties of the crack surfaces in order to compare them with those of other experiments, in which this kind of studies have been done on different materials.

The paper is organized as follows: in Section 2 the experimental apparatus is described; in Section 3 the velocity measurements are reported. In Section 4 the surface properties are discussed. The connection with sound measurements is analysed in Section 5. The crosscorrelation among the different signals is studied in Section 6. The statistical features of the surface profile are described in Section 7. Finally conclusions are given in Section 8.

2. Experimental Apparatus

The experimental apparatus consists of a tensile machine which can apply a maximum force of about 23000 N. The machine is driven by a stepping motor which allows us to make deformation

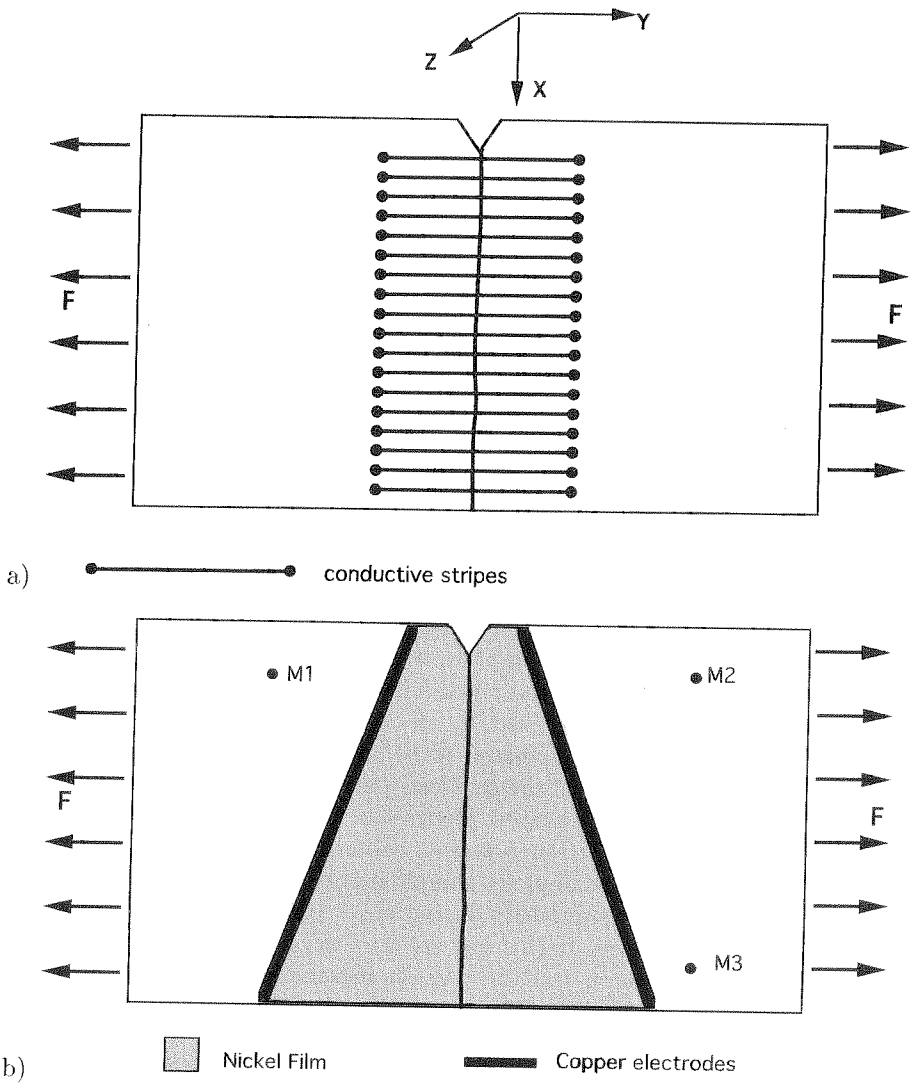

Fig. 1. — Schematic drawing of a typical sample. a) Conductive stripes used for calibration. b) Conductive thin film. Locations of the ultrasound detectors (M1, M2, M3) are also indicated. The x axis is the direction of propagation of the crack and the stress is applied along y.

increments of less than 1 μm. The machine is installed on an optical table to perform optical measurements on the sample. The whole apparatus is surrounded by a Faraday screen. We measure the force F applied to the sample, the velocity of crack propagation, the sound emission produced before and during fracture. Finally we study the roughness of the surfaces generated by the crack.

Experiments have been done using cell-cast plexiglas (PMMA) (a few checks have been done also in glass). We used different kinds of PMMA, with density $\rho = 1200$ kg/m^3 and various Young moduli E, specifically 1.6×10^9 N/m^2 $\leq E \leq 3.2 \times 10^9$ N/m^2. A drawing of a typical sample is shown in Figure 1. The samples have a rectangular shape of length $L = 29$ cm and

a height $H = 10$ or 20 cm. The sample thickness b varies from 1 mm to 10 mm to verify whether the features of the crack instability are independent of the sample thickness. Thus the only quantity kept fixed in the geometry of our experiment is the sample width L. Four thick plates were glued on the sample sides in order to install it in the computer-controlled tensile machine. To initiate the fracture just in the center of the sample long side, an initial cut l_c, which was always between 5 and 10 mm, was done at $L/2$. The length and the shape of this cut determine the dynamical properties of the crack. Long cuts with a very sharp tip produce in general slow speed cracks whereas cuts with an initially rounded tip usually generate very fast cracks. Fracture is performed by applying force in the plane of the sample and parallel to the longest side of the plate (mode I crack [1]).

The velocity $V(t)$ of a crack is measured using two different techniques. One is based on conductivity measurements of several (usually 19) equally spaced conductive stripes (see Fig. 1a), deposited on one of the two surfaces of the sample, which are cut by the propagating crack. When a stripe is cut a pulse is detected by a suitable electronic circuit. However this technique gives the crack length $l(t)$ only at 19 points thus we use also another method, which although less accurate, allows us to measure $l(t)$ continuously. The method is similar to that of references [3,4] and it consists in measuring the resistance of a thin conductive film deposited on the other surface of the sample to be cracked, Figure 1b. On the two sides of the film two electrodes are glued with a conductive glue. The resistance, measured between the two electrodes, is initially of about 1 Ω and it increases when the crack propagates between the two electrodes. These electrodes are inclined in order to reduce the non-linearity of the dependence of the film resistance as a function of the crack length l. This resistance is measured by the Wheastone bridge whose output is digitized, by an oscilloscope LeCroy 9430, at 100 MHz rate with 10 bits accuracy, which can be increased to 13 bits by reducing the bandpass to 1 MHz. Furthermore using the two channels of the oscilloscope at two different amplifications the very beginning of the crack is precisely measured. Because of the non-linearity of the film resistance *versus* the length of the crack the system has been calibrated by cutting the resistive film with a knife. Since the film varies from sample to sample it is rather useful to check the calibration of the continuous resistance measurements during crack propagation by the reference pulses produced by the conductive stripes. In this way the accuracy of the method used in reference [3] is greatly improved. The maximum sensitivity in the measurement of $l(t)$ is less than 0.05 mm and the absolute accuracy about 5%. The speed $V(t)$ is obtained by the derivation of $l(t)$. To compute the derivative of the signal $l(t)$ we use several methods to check the influence of the measurement noise on the result. No appreciable difference has been found. The speed resolution is between 5 m s^{-1} and 20 m s^{-1} depending on the bandpass.

The sound emission, produced by the moving crack, is measured in the range 10 kHz, 1 MHz (Pinducer, and Matec) with several wide band microphones located on the plate surfaces at about 5 cm from the tip of the initial cut. The microphones location is indicated in Figure 1a.

Also several optical measurements have been performed. The local sample strain is measured using the deflection of a laser beam which passes through the sample close to the region where the crack will propagate (see Fig. 1). When the sample is deformed the laser beam is deflected because of the sample deformation and this deflection is measured with a positon sensitive detector (UDT200). This measurement is useful to know the relaxation time of the sample during crack propagation.

Experiments are done by increasing the sample strain, till the fracture point, by fixed increment steps of less than 100 μm for plexiglas and 10 μm for glass samples. The strain rate is less than 10 μm/s. Between two consecutive steps we wait about 10 s, and crack usually occurs during this waiting time. The force F corresponding to the applied strain is continuously

monitored. We would like to point out that a careful optical analysis of the stress field of the sample shows that no relaxation occurs in the sample till the moment in which the fracture is passed close to the measuring point. This indicates that crack is propagating with a constant applied stress. Once a sample is broken the profile of the fracture surfaces is studied with an optical profilometer [17]. The surface height $h(x, y)$ is sampled at a 10 μm rate on a two-dimensional array constituted by 50 lines of 10^4 points each. The lines are parallel to the direction of the crack propagation (x axis) and are separated by a distance of either 10 or 50 μm depending on the plate.

3. Crack Length and Speed as Function of Time

As an example of the experimental results on cell-cast PMMA samples we show in Figure 2a a typical plot of the crack length *versus* time and in Figure 2b the expanded view of the beginning of the crack propagation. From these figures one can see that the noise is less than 0.05 mm, which is the resolution of the measurement. Typical plots of the crack speed $V(t)$ as a function of time or length are shown in Figure 3. Looking at the very beginning of these curves one sees that the rms noise of the speed is about 10 m/s. It is important to notice that in general the samples present a velocity jump at the beginning of the crack propagation as can be seen in Figures 3a, c, d. This agrees with the result of references [3] and [7]. However we have found a few cases where the crack begins with a smooth acceleration. We do not know where this difference comes from but it is interesting to show that the beginning of the propagation can have another behaviour than a velocity jump. The curves in Figures 2 and 3 correspond in this case to samples having the same elastic properties and the same sizes. However the fracture dynamics and the steady state speeds V_f are clearly very different from one crack to another. Notice the presence, in the curves of Figures 3b, 3c, 3d, 3e, of a strong increase of the velocity fluctuations above a certain velocity. This effect has been also described in references [3, 4], and we will discuss this point in Section 5.

Let us consider for the moment just the crack steady state speed V_f. In Figure 3e the velocity is plotted *versus* l for the fastest sample which show that for $l > 5$ cm the mean crack speed is in a steady state regime. Thus in general for 5 cm $< l < L$ one can consider the crack properties in a steady state regime. We found that V_f follows a well defined law as a function of the stress of the sample during the crack propagation. If F_c is the force necessary to start the crack propagation in the sample, then the corresponding stress is $P = F_c/b$ and the corresponding strain is $\Delta = P/E$, where E is the Young modulus. For the plots shown in Figures 3a, b, c and d $[\Delta \times 10^{-3}]$ was 2.71, 2.80, 6.17, 6.45 respectively. The samples from Figure 3 have the same elastic parameters, $E_o = 2.5 \times 10^9$ N m^{-2} and $V_R \simeq 870$ m/s (see Appendix), thus as we have already mentioned, the different final speeds have been obtained only by changing the length and the shape of the initial cut.

In Figure 4 we show V_N^2 measured on several samples as a function of the corresponding $1/\Delta$, where $V_N = V_f/V_R$. We see that all the points are almost aligned on a straight line which suggests that in a first approximation:

$$V_N \simeq V_o \cdot \sqrt{1 - \frac{\Delta_{min}}{\Delta}} \tag{1}$$

with $V_o \simeq 0.88$ and $\Delta_{min} \simeq (2.35 \pm 0.12) \times 10^{-3}$. Equation (1) shows the dependence on Δ similar to that of the equation proposed by Langer in reference [11] in the case of viscous dissipation. It is also coherent with several other theoretical results [9] which predicts that the highest velocities of propagation are reached only with a very large strain of the samples.

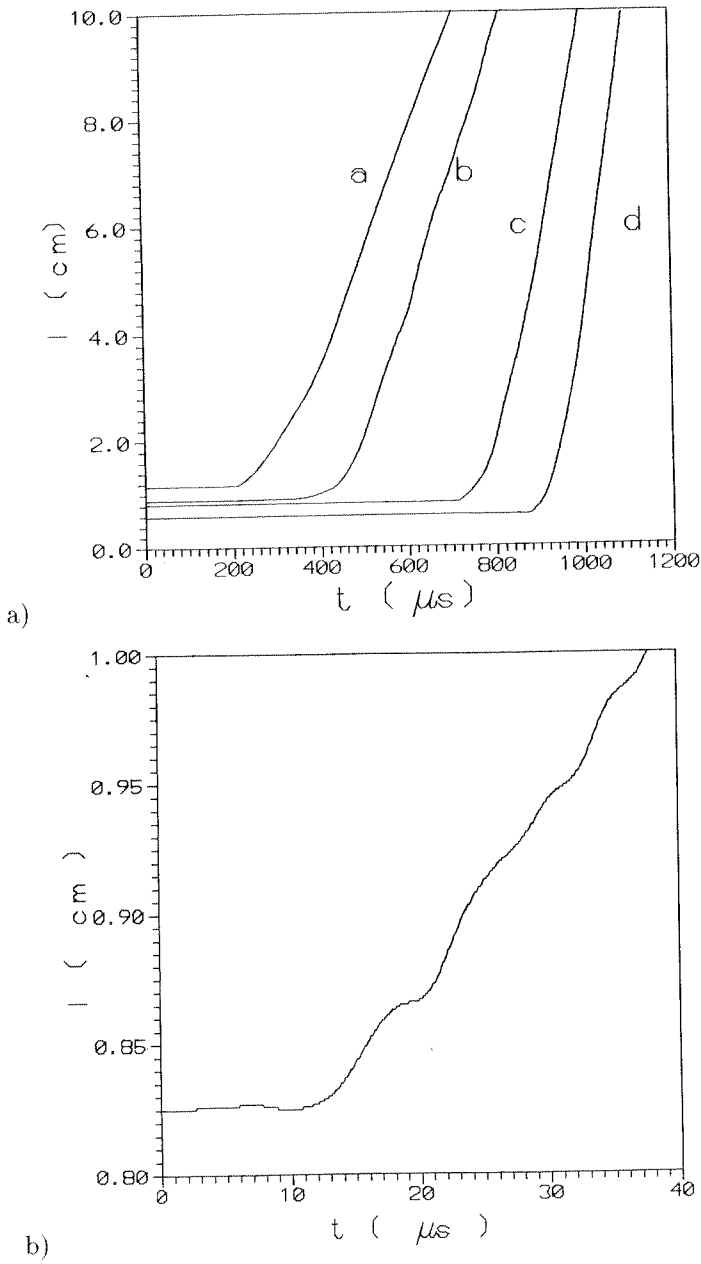

Fig. 2. — a)The crack length *versus* time measured in four different samples. The dynamics are clearly different from one sample to another. b) Expanded view of the very first instant of the curve d.

One can also study the initial mean acceleration a of the crack which we define as $a = 0.5V_f/t_a$ where t_a is the time needed to the crack to reach $0.5V_f$. This acceleration is made dimensionless in the following way $\hat{a} = a\ L/V_R^2$. The dimensionless acceleration $\hat{a}$ turns out to be a function of the following parameter $\hat{\Delta} = \Delta\ (L/l_c)$. This parameter takes roughly into account the shape

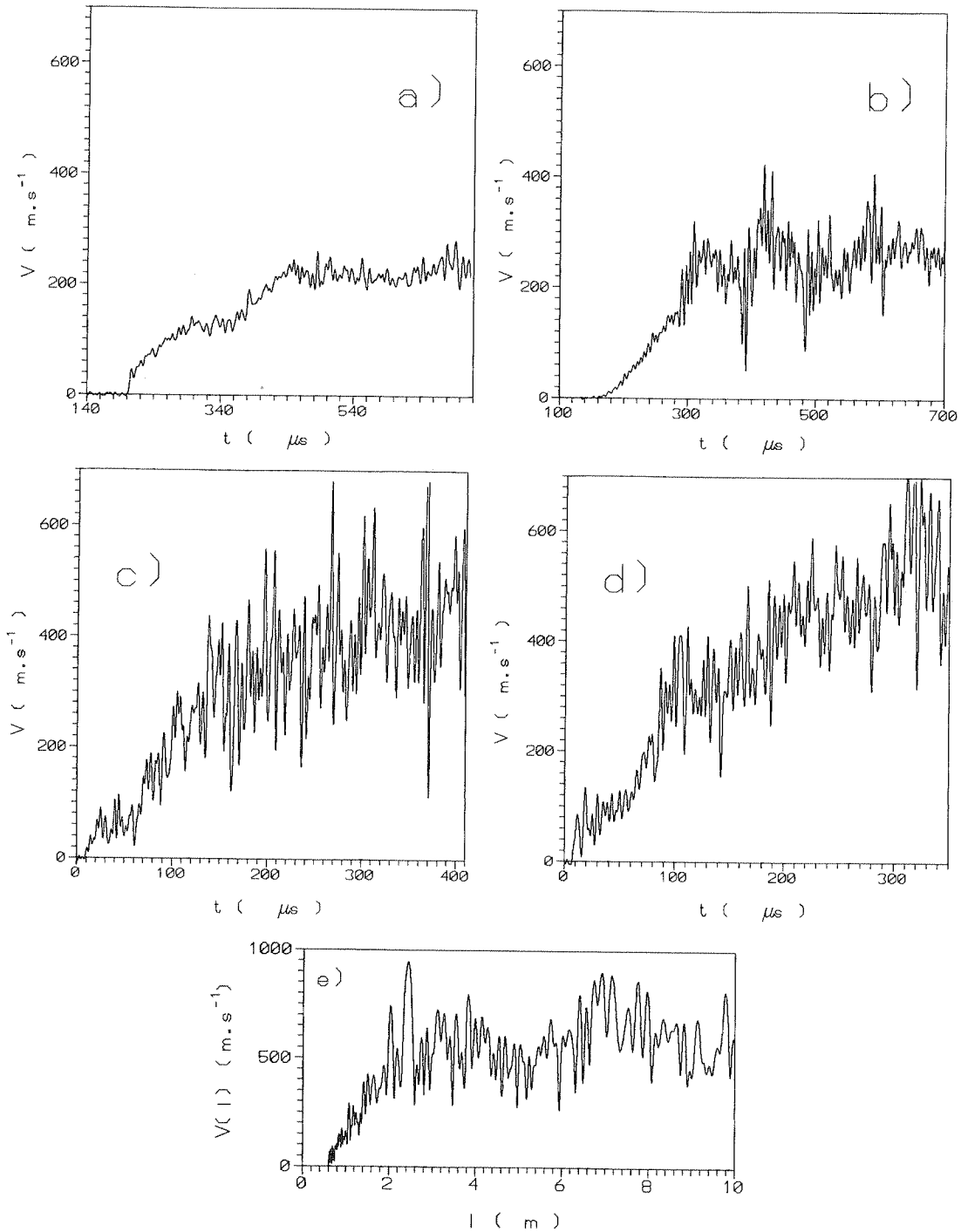

Fig. 3. — Local velocity of the crack *versus* time measured in the four samples a, b, c, d shown in Figure 2a where the final speed V_f reached different values. Respectively $V_f = 200$ m/s in a), $V_f = 250$ m/s in b), $V_f = 450$ m/s in c) and $V_f = 580$ m/s in d). e) Local velocity *versus* length, for a sample with $V_f = 630$ m/s. Notice that for $l > 5$ cm the mean velocity is in a steady state regime.

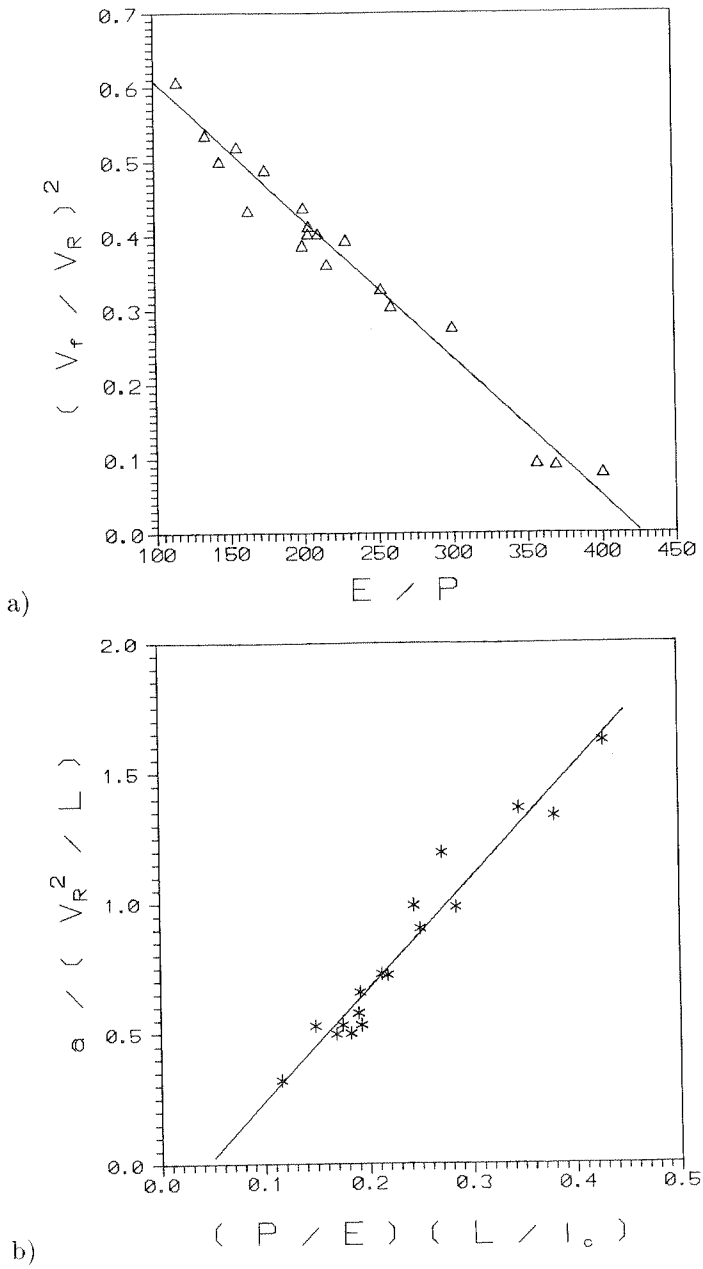

Fig. 4. — a) Square of the steady state reduced velocity V_f/V_R of the crack as function of the inverse sample strain Δ^{-1}. b) Dimensionless initial acceleration aL/V_R^2 of a crack as a function of the normalized strain Δ (L/l_c).

of the notch. Indeed two notches of equal l_c, in samples with equal L, may produce cracks with a completely different dynamics, depending on the shape of the notch tip. A crack with a given l_c and a blunted notch will require a big Δ in order to start, whereas a crack with the

same l_c and a very sharp notch will start at small values of Δ.

In Figure 4b, $\hat{a}$ is drawn as a function of $\hat{\Delta}$. We see that all the points are aligned almost on a straight line. This suggests that the following relationship is approximately satisfied

$$a \frac{L}{V_R^2} \simeq A \Delta \frac{L}{l_c} + B \tag{2}.$$

with $A = 4.2 \pm 0.2$ and $B = -0.17 \pm 0.01$ One can find from equation (2) that $a = 0$ for $\Delta = \Delta_{min}$ and $l_c = l_{max} \simeq (1.8 \pm 0.4)$ cm.

Using these measured values, one can compute the minimum surface energy release rate G [1]. According to Irwin the initial energy release rate G [1] in our samples is:

$$G = \frac{\pi p^2 l_c}{E} \tag{3}.$$

From the fit of the data in Figures 4a, b with equations (1) and (2) one finds (fixing $l_c = l_{max}$ in Eq. (2)), that the minimum value of Δ in order to have a $V_f \simeq 0$ and $a \simeq 0$ is Δ_{min}, therefore $p_{min} = \Delta_{min} E$. Inserting this value in equations (2) and (3) one can compute the minimum G. We obtain, for $E = 3 \times 10^9$ N/m^2, $G = G_1 = (937 \pm 327)$ J/m^2 and for $E = 2 \times 10^9$ N/m^2, $G = G_2 = (624 \pm 218)$ J/m^2 which are close to the values reported in literature [2, 19] for measurements with $V_f \simeq 0$. From the Griffith criterion one gets for the surface energy T of PMMA either $T = G_1/2 \simeq (468 \pm 163)$ N/m^2 or $T = G_2/2 \simeq (319 \pm 109)$ N/m^2. These values are roughly in the range of the values of refererence [2] ($T \simeq 144$ J/m^2) for $V_f \simeq 0$. This is interesting because extrapolating the fits of our experimental data obtained at high V_f we can roughly estimate the value of T at velocities close to zero.

4. Surface Properties

The possibility of having various final speeds is very useful because the steady state velocity V_f is a very important control parameter which determines the properties of the crack. The most striking of these properties is the profile of the surfaces produced by the crack. However, as we will see in this section, not only V_f is an important control parameter but also the local velocity $V(t)$. Indeed, depending on $V(t)$, the crack surfaces can be smooth or rough. This is shown in Figure 5 where typical profiles $h(x, y)$ of the crack surfaces are reported as a function of the crack length at fixed y.

In Figure 5a we see that at $V_f = 260$ m/s the surface is smooth. In contrast at $V_f = 580$ m/s, Figure 5b, the roughness begins to develop. Finally at $V_f = 670$ m/s, Figure 5c, the surface is very rough. From these measurements one deduces that if $V(t)$ is smaller than a certain threshold value V_c the surface of the crack is completely smooth. This local dependence can be quantitatively studied using the local roughness $R(l)$, that is the rms amplitude of the surface profile measured on intervals of 0.5 cm centered at the point l of the crack profile. $R(l)$ obtained this way for each profile parallel to the crack direction is then averaged on the y direction.

As an example the rms amplitude of the profile of the same sample shown in Figure 5b, is presented in Figure 6 as a function of l. The corresponding mean velocity $V_m(l)$, that is the average of $V(l)$ on 0.5 cm intervals, is also shown. We clearly see that $R(l)$ is zero for $V(l)$ smaller than $V_c \simeq 0.5 V_R$ whereas it grows when $V(l)$ increases, indicating that $R(l)$ is a function of the local speed.

This result is demonstrated in Figure 7a where $R(l)$ is plotted *versus* $V_m(l)$ for 10 different samples. All the data collapse almost on the same curve. The values of $R(l)$ are close to zero for $V_m(l) < 0.5 V_R$ and increases for $V_m(l) > 0.5 V_R$. This is seen much better in the expanded

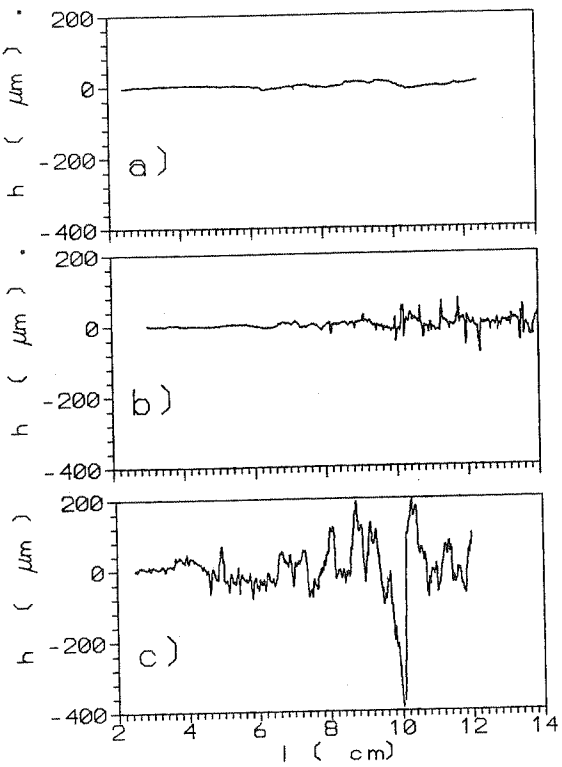

Fig. 5. — Surface profile $h(x, y)$ produced by the crack as a function of the crack length l at fixed y. In a) the steady state crack speed V_f was 250 m/s whereas in b) and c) $V_f =$ 580 m/s and $V_f = 670$ m/s respectively.

view of Figure 7a, which clearly shows a sharp transition at $V_m(l) \simeq 0.5V_R = 450$ m/s. The maximum roughness R_{max} is a function of the steady state velocity V_f. This can be seen in Figure 7b where R_{max} is plotted as a function of V_f. Here also we see that for $V_f < 450$ m/s the roughness is almost zero and begins to rapidly increase for $V_f > 450$ m/s. At this point we would like to emphasize that the data, presented in the expanded view of Figure 7a, show that a slight deviation from the noise level occurs at $V > 330$ m/s, or $V_u \simeq 0.32V_R$. This threshold is consistent with the value of microbranching reported in reference [18]. It has to be pointed out that microbranches propagates mainly inside the volume and give just small perturbations on the surface. For this reason they cannot be clearly detected by a standard profilometer, which measures the surface height. Indeed, using a microscope, we checked that several microbranches begin to appear for $V > V_u$. As we will see in the next section this threshold $V_u \simeq (0.32 \pm 0.04)V_R$ is also the threshold for the velocity oscillations and a weak continuous sound emission. In contrast $V_c \simeq 450$ m/s is the threshold at which the strong roughness, associated with a strong sound emission (see next section) begins to develop. Further the well known phenomenon [1] of macrobranching takes place at even higher local velocity at about $V_b = 0.65 \cdot V_R$. The latter occurs just for the fastest cracks with $V_f = 0.75 \cdot V_R$, when a sufficiently large strain is applied to the sample.

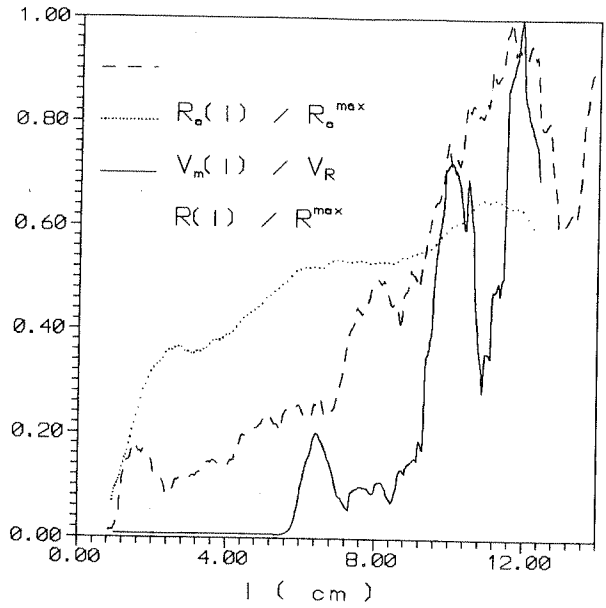

Fig. 6. — Local reduced rms values, normalized to its maximum, of sound emission $R_a(l)$ (dashed line), of the surface profile $R(l)$ (continuous line) and mean local velocity $V_m(l)$ (dotted line) as a function of l, measured in the sample with $V_f = 580$ m/s.

5. Sound Emission and Velocity Oscillations

The other important phenomenon which appears during fracture is sound emission [4]. The sound amplitudes is measured by the microphones, described in Section 2, in terms of $d = ds/dt$, where s is the local displacement induced by the sound wave on the sample surface. Examples of sound signals, measured in terms of the displacement speed d, recorded during the three fracture experiments of Figures 3a, b and d are shown in Figures 8a, b and c respectively. The sound amplitude and waveform are also found to be a function of $V(t)$. We see that in Figure 8a there is just a pulse and then sound relaxes almost to zero whereas in Figures 8b and c the sound emission continues after the first pulse. The maximum sound energy found in the fastest cracks, corresponds to about 1.5 J/m^2 which is roughly 1% of the minimum surface energy T. To study quantitatively the relationship between the sound amplitude and $V(l)$ we measure the local rms amplitude $R_a(l)$ of the sound signals on time intervals of about 1 cm/$V_m(l)$. $R_a(l)$ (normalized to its maximum) is shown in Figure 6 together with the corresponding reduced values of $V_m(l)$ and $R(l)$. We note that the sound emission remains weak till the point where $R(l)$ begins to increase, therefore the onset of roughness is associated with a strong sound emitted by the propagating crack [4]. We have also found that no sound emission occurs in PMMA before that the speed $V_s = (120 \pm 10)$ m/s is reached. This can be observed in Figure 7c where $R_a(l)$, measured in four different samples, is presented as a function of $V_m(l)$ (lines). The inset in the figure is an expanded view of the beginning of the plot. One can clearly see that below 100 m/s the rms is zero and above this value there is a sharp transition. The rounding of the rms curves around 100 m/s is just due to the fact that $R_a(l)$ is measured on 1 cm/$V_m(l)$ intervals. The sound emission begins to continue after this first pulse for $V_m(l) > V_u$ which is the threshold defined in the previous section. However

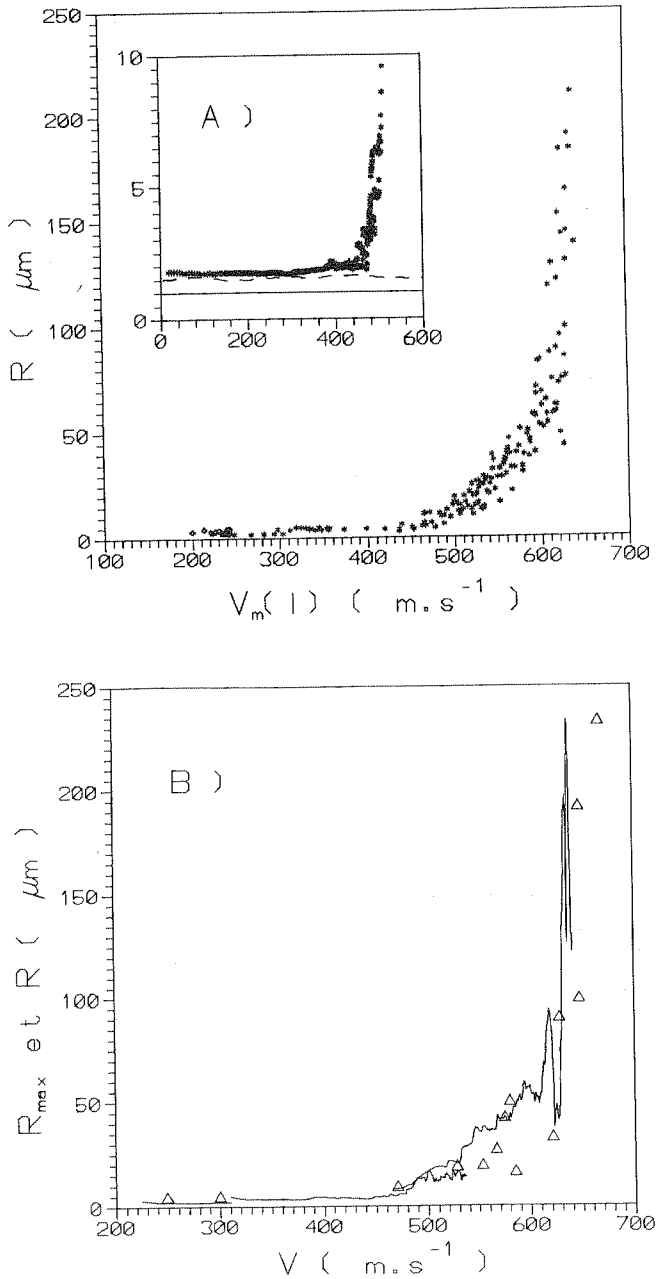

Fig. 7. — a) Local rms $R(l)$ of $h(x, y)$ as a function of the mean local velocity $V_{\rm m}(l)$. The inset is the same in the extended scale in the vicinity of the instability. b) Maximum rms $R_{\rm max}$ as a fonction of the final speed. c) Local rms $R_{\rm a}(l)$ of the sound amplitude as a function of $V_{\rm m}(l)$ (lines) for four different plates having different $V_{\rm f}$. Specifically $V_{\rm f} = 210$ m/s (long dashed line) $V_{\rm f} = 240$ m/s (short dashed line), $V_{\rm f} = 580$ m/s (continuous line) and $V_{\rm f} = 670$ m/s (dotted line). The symbols (o) represent the maximum rms of the sound amplitude as a function of $V_{\rm f}$ for several samples. The horizontal dashed line is the sound level at $V_{\rm c}$. The insert is an expanded view in the vicinity of the instability. d) Local rms of the mean velocity oscillation, measured in the steady state, as a function of $V_{\rm f}$.

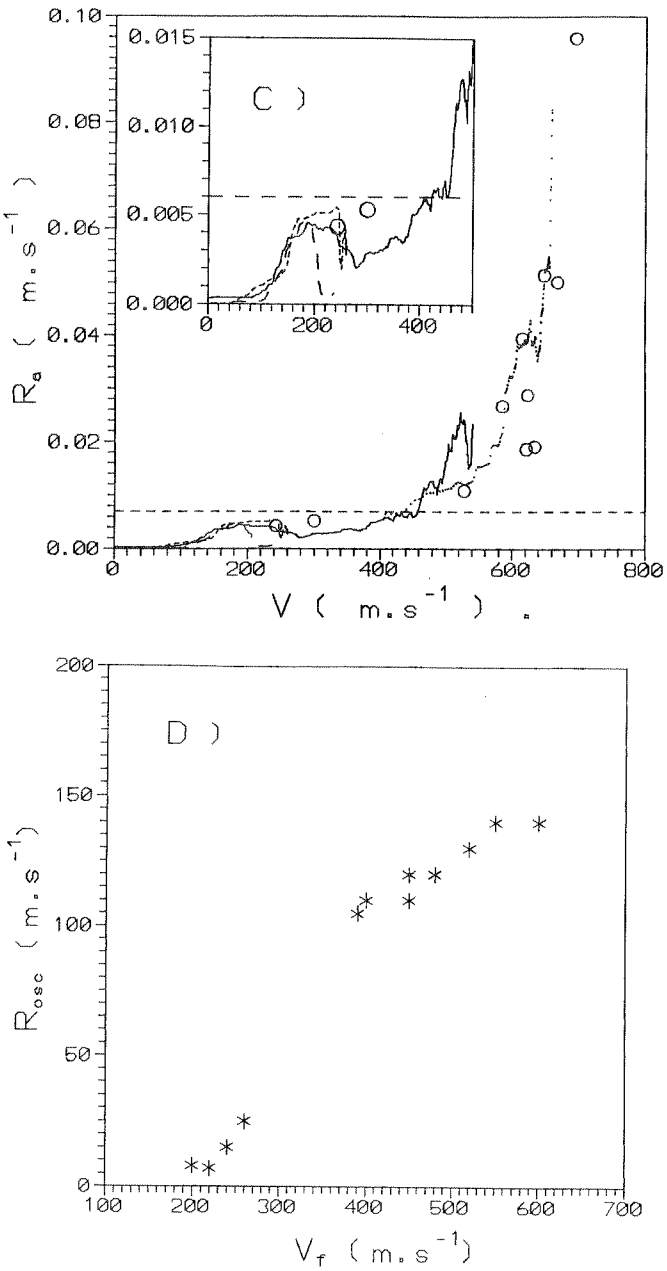

Fig. 7. — *(Continued.)*

for $V_u < V_m(l) < 0.5V_R$ we see that $R_a(l)$ is weak whereas it begins to rapidly increase for $V_m(l) > 0.5V_R$. We would like to point out that the maximum rms of sound emission, shown in Figure 7c as a function of V_f (circles), has the same functional behaviour. Indeed we clearly noticed that the sound level is weak for $V_f < 0.5V_R$. This means that the sound emission increases when the surface becomes rough, as suggested in reference [4].

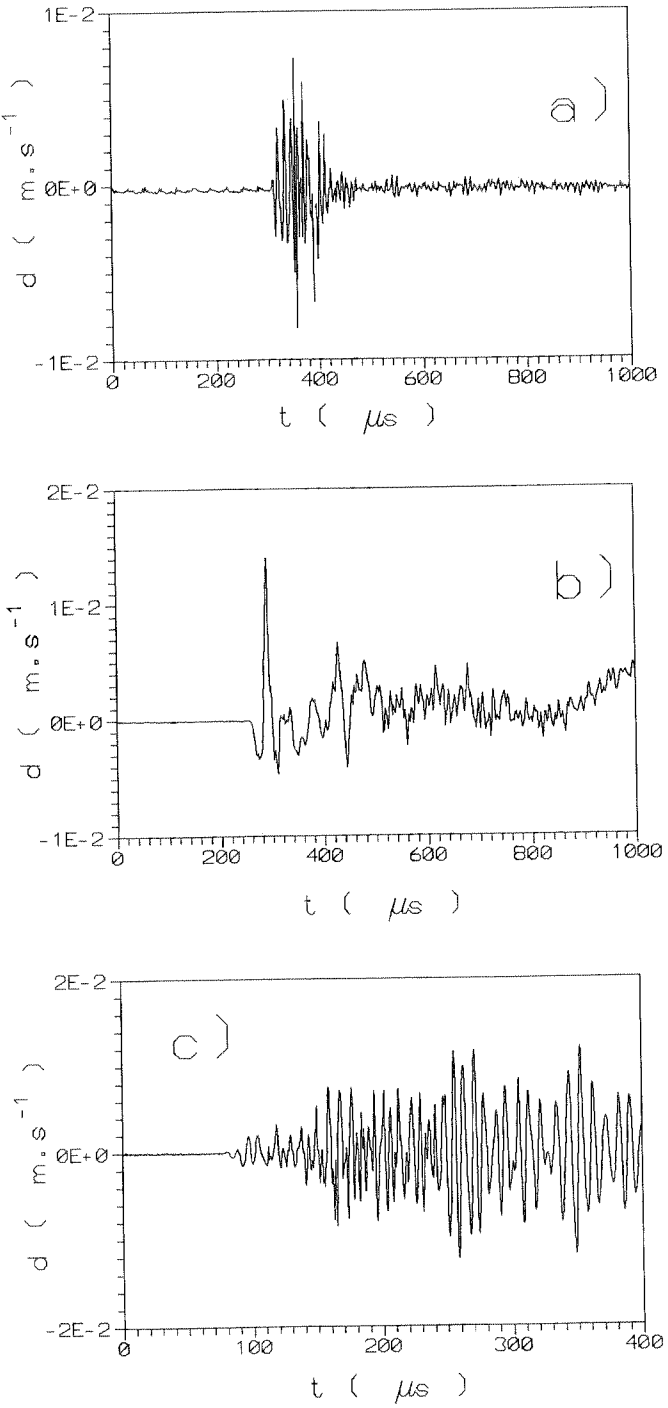

Fig. 8. — Sound emission, measured in terms of dispacement speed d, as a function of time for three cracks shown in Figure 3. a) $V_f = 200$ m/s as in Figure 3a. b) corresponds to Figure 3b $V_f = 250$ m/s and c) to Figure 3d $V_f = 580$ m/s.

Furthermore we observe as in references [3, 4] velocity fluctuations when the velocity of the crack increases. Indeed in Figures 3b, c, d, we see that the oscillations around the local mean velocity are larger than at the very beginning where the curve $V(t)$ is rather smooth. This must be compared with the slow crack of Figure 3a, where oscillations are very weak. The final speeds of the two cracks in Figures 3a and b, are $V_f = 200$ m/s and $V_f = 250$ m/s respectively. In both samples the crack surfaces are completely smooth but one does not show velocity oscillations whereas another shows clearly an increase of the velocity fluctuations. Furthermore also the properties of sound in these two samples are different as it can be seen in Figures 8a and b where the sound emission recorded during the two slow cracks are shown in Figures 3a, b, is presented. In Figure 8a, corresponding to Figure 3a, the sound consists of a short pulse emitted just at the very beginning of the crack at $V(l) > V_s$. In contrast in Figure 8b, corresponding to Figure 3b, the sound emission continues during crack propagation when the velocity oscillates, here $V_f \simeq V_u$. However the maximum amplitude of this sound emission is rather small and falls below the horizontal dashed line (sound level at $V_m(l) = V_c$) in Figure 7c. Here we can also notice that $R_a(l)$, corresponding to the slowest crack, decreases after the first spike. Thus one concludes that the velocity oscillations are not necessarily related to the roughness, as it has been proposed in references [3, 4]. However as it can be noticed in Figures 8c and 7c the sound emission becomes very strong when the sample is rough.

The same occurs for the velocity oscillations r.m.s R_{osc} which is also a function of the steady state velocity V_f. This is shown in Figure 7d where R_{osc}, measured in the steady state regime, is reported as a function of V_f. We clearly observe that R_{osc} is close to zero for $V_f < V_u$ and begins to increase for $V_f > V_u$. The four plots in Figure 7 are very useful to understand that although the local properties of the crack are controlled by the local velocity $V(l)$, the mean properties (rms of the roughness of the velocity oscillations and of the sound emission, measured in steady state) are controlled by the steady state velocity V_f.

6. Cross Correlations

The cross correlation between the different quantities allows us to clarify the relationships between sound emission, velocity oscillations and surface roughness. The cross correlation $C(\delta)$ between $h(l, y_o)$ and $V(l)$, in the steady state regime, computed for the crack with $V_f = 580$ m/s, is shown in Figure 9a as a function of the distance δ. We see that the maximum correlation is about 0.3 which is consistent with the values reported in reference [3]. The mean oscillation period is about 3 mm, which is close to the characteristic length of the surface asperities. Thus the correlation between velocity and roughness is rather low. In Figure 9b we show the sound-velocity correlation as a function of the delay time τ for a crack with $V_f = 580$ m/s. In this case we see that the correlation of the order of 0.5 is higher than that between velocity and roughness.

However this is not the best way to measure the cross correlation between sound and velocity, because the sound emitted at the crack tip takes a certain amount of time to go from the source to the detector and it is attenuated along the acoustic path. Therefore these two effects have to be taken into account to correctly compare $S(l)$ and $V(l)$. Assuming that the maximum sound emission occurs at the crack tip, which is moving at $V(l(t))$. If the sound detector is located at $x_o = 1$ cm, $y_o = 2$ cm (see Fig. 1) then the sound emitted at the location $l(t)$ will take a time $\delta t = [\sqrt{(l(t) - x_o)^2 + y_o^2}]/V_R$ to reach the microphone. Thus we corrected the received sound signal $S(t)$ by shifting the time origin, that is $S'(t) = S(t - \delta t)$. By inverting the measurement of $l(t)$ one can express t as a function of l and evaluate $S'(l)$ which is shown in Figure 10a. Then the cross correlation between $V(l)$ and $S'(l)$ can be computed and the result is shown in Figure 10b. We see that the correlation is about 0.8. However the cross correlation is not the

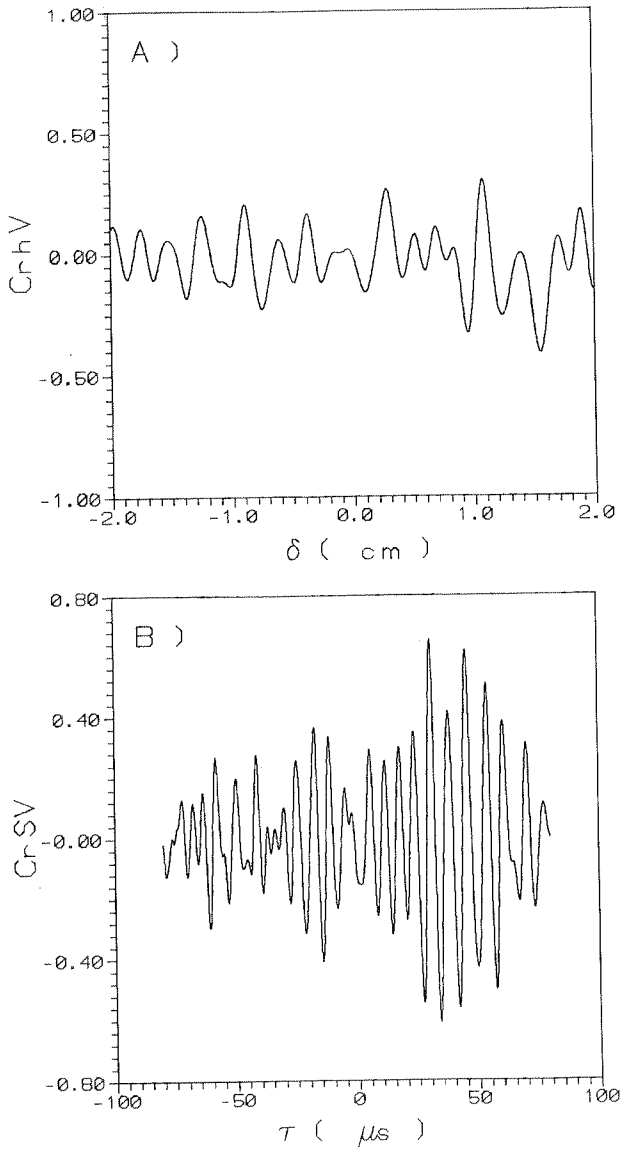

Fig. 9. — a) Cross correlation between the velocity $V(l)$ and $h(l, y)$ as a function of the distance δ. b) Cross correlation between sound $S(t)$ and velocity $V(t)$ as a function of τ for a rough crack ($V_f = 580$ m/s).

best technique in order to study the correlation between signals with very broad spectra like those of $S(l), V(l)$ and $h(l)$. It is much better to look at the coherence function between two signals which is defined [20]:

$$\mathrm{Ch}_{1,2}(K) = \frac{|\langle F_1(K)\ F_2^*(K)\rangle|}{\sqrt{\langle|F_1(K)|^2\rangle\ \langle|F_2(K)|^2\rangle}} \tag{5}$$

where F_i is the Fourier transform of the signal i (F_i^* is the complex coniugate) and $\langle ....\rangle$

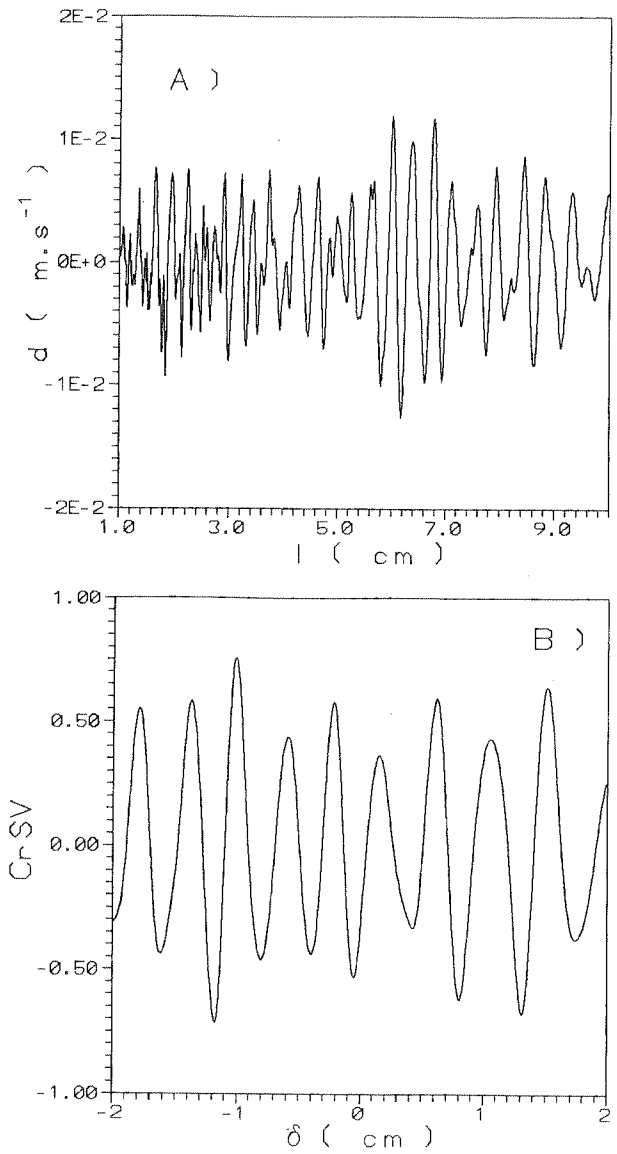

Fig. 10. — a) Sound signal $S'(l)$ as a function of l for cracks with $V_f = 580$ m/s. b) Cross correlation between $V(l)$ and $S'(l)$ as a function of δ in a crack with $V_f = 580$ m/s.

stands for ensemble average. Of course Ch is one (zero) for wavevectors where the signals are correlated (uncorrelated). In order to compute the sound velocity coherence $\mathrm{Ch}_{S,V}$ (or of profile velocity coherence $\mathrm{Ch}_{h,V}$), we have calculated the Fourier transform of $S(l)$ and $V(l)$ over many windows (2 cm wide) centered in different locations l and then we have performed the averages indicated in equation (5) over all the windows. The results of this analysis, shown in Figure 11, confirms the results of the correlations. The $\mathrm{Ch}_{S,V}$ (Fig. 11a) is 1 for a wavelength $\lambda \simeq 1$ mm whereas $\mathrm{Ch}_{h,V}$ (Fig. 11b) is never higher than 0.6 at $\lambda \simeq 3$ mm. Thus the maximum correlations of the signals also occurs for different wavelength.

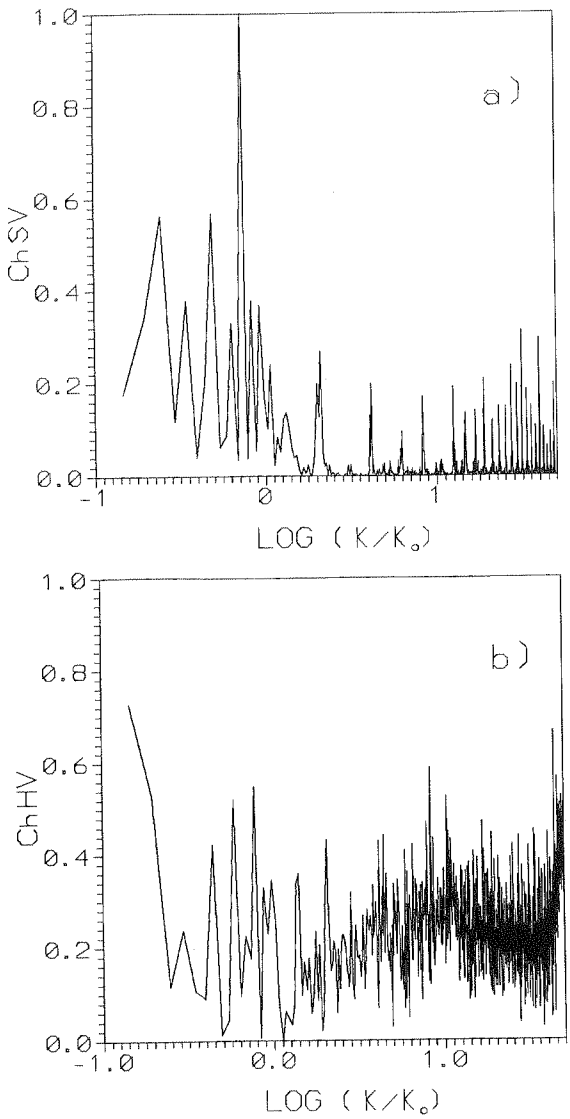

Fig. 11. — a) Sound-velocity coherence function and b) profile-velocity coherence measured in a sample with $V_f = 580$ m/s. ($2\pi/K_o = 1$ mm)

The coherence functions show that the sound and velocity oscillations are very correlated even in the case when no roughness is present. In contrast the velocity oscillations and the roughness are weakly correlated. Thus one can argue that either is the appearance of roughness which is producing a strong sound emission or the strong increase of sound emission observed for $V > V_c$ can be at the origin of the roughness. However this point requires further theoretical and experimental verification in order to be clarified.

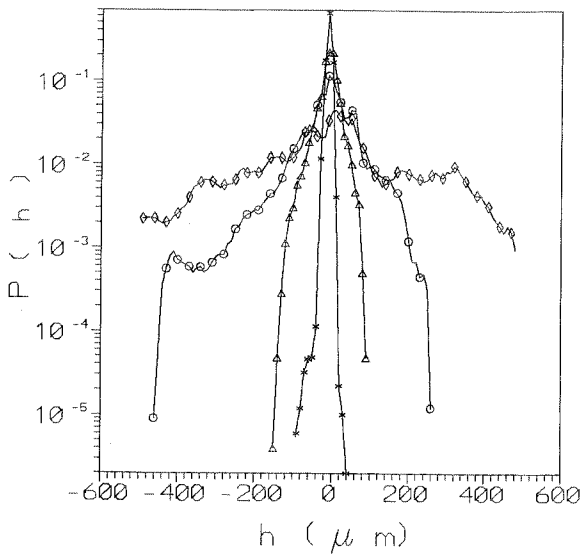

Fig. 12. — Probability distribution function of $h(x, y)$ measured in different samples with various final velocities. $(*)V_f = 250$ m/s, $(\triangle)V_f = 580$ m/s, $(\bigcirc)V_f = 668$ m/s and $(\diamond)V_f = 650$ m/s.

7. Statistical Features of the Surface Profile

Finally we would like to discuss some statistical features of the roughness. As we have seen in Figure 5 the surface topography produced by the crack, changes significantly as a function of V_f. Therefore one is interested in knowing whether also the probability distribution functions $P(h)$ of the surface height h are influenced by the propagation speed. In Figure 12 we show $P(h)$ *versus* h measured on several samples where the crack reached different V_f. Of course these statistical features are studied in regions where the crack speed is almost in a steady state.

We see that $P(h)$, measured on a sample with $V_f = 250$ m/s, is narrow with a broadening equal to the profilometer instrumental noise. At $V_f = 580$ m/s the broadening is much larger, that indicates the increase of roughness at the velocity bigger than V_c. Furthermore the shape of $P(h)$ is changed by the appearance of large tails .

At $V_f = 650$ m/s, $P(h)$ is even broader, the tails are very wide, so h is almost uniformly distributed. Usually PDF with very wide tails are associated with very intermittent signals (the profile h in our case) as for example in fully developed turbulence [21]. It means that strongly deviating events from an average have here a significant contribution into statistics unlike, *e.g.*, Gaussian distribution where their contribution is exponentially small. From this measurement one deduces that because of the strong deviation from a Gaussian of $P(h)$ for high V_f the low order moments of the distribution are not sufficient to characterize the PDF of h, as it is usually done but also the skewness and the flatness are important. Incidentally we want to stress that also the sound emission and the velocity PDF present broad tails.

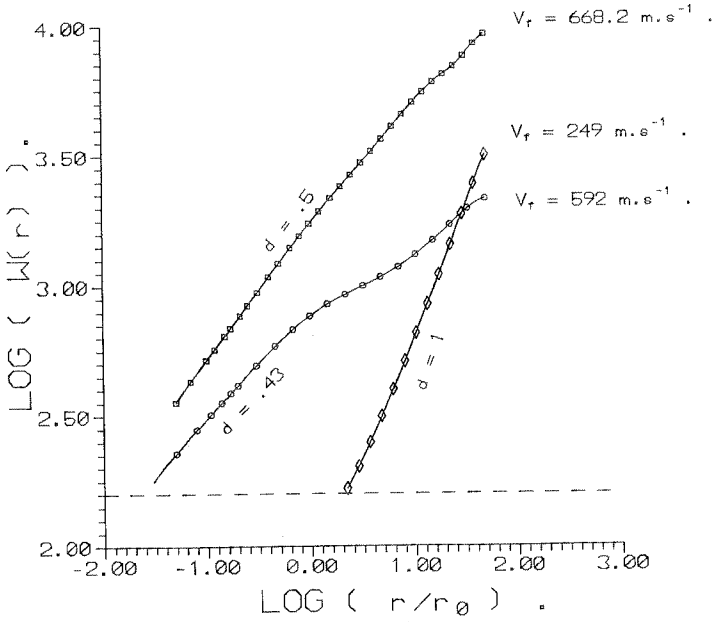

Fig. 13. — $W(r)$ defined in equation (3) is plotted as a function of r (r_o = 1 mm) for samples with different final velocities.

The surface topography is often characterized [22] by the roughness $W(r)$ that is the rms of $h(x, y)$ measured on intervals of size r. Specifically

$$W_x(r) = \sqrt{\left\langle \int_x^{x+r} h^2(x', y)\mathrm{d}x' - \left[\int_x^{x+r} h(x', y)\mathrm{d}x'\right]^2 \right\rangle_x} \tag{6}$$

where $\langle ... \rangle_x$ stands for average over the variable x. The function $W(r)$ is found to be a power law of r, that is $W(r) \propto r^\alpha$. The exponent α in the literature is associated with the multiaffine properties of surfaces. In the three-dimensional case and in many different materials, α is found to be 0.8 if x (in Eq. (6)) is transverse to the crack direction and it takes a different value (about 0.7) if x is parallel to the crack [23]. The exponent α is about 0.7, also in quasi two-dimensional materials, where the crack is almost a line and not a surface. Because of the small thickness of our samples we have measured $W(r)$ along x (the crack direction in our experiment) and then we averaged the results along y. We find that $W(r)$ is a function of the steady state velocity V_f as we have seen that the crack profile is a function of V_f. This can be seen in Figure 13 where $\log W(r)$ measured for three different samples, is drawn as a function of $\log r$. The slopes of the curves are very different as a function of V_f. Of course $\alpha \simeq 1$ for smooth surfaces and reaches the value 0.5 for the fastest and roughest crack. The exponent is close to that of the Brownian motion except that here the distribution of $h(x, y)$ is not Gaussian. This exponent is smaller than that found for $W(r)$ in directions parallel to the fracture in other materials. We have checked the statistical accuracy of this exponent by looking at the power spectrum $S(k)$ of $h(x, y)$ which is reported in Figure 14a. We clearly see that there is a region where the spectrum decreases as K^{-2} which is consistent with the exponent $\alpha \simeq 0.5$. This exponent is considerably smaller than that found in other materials which is 0.8 [22–25]. The reasons for

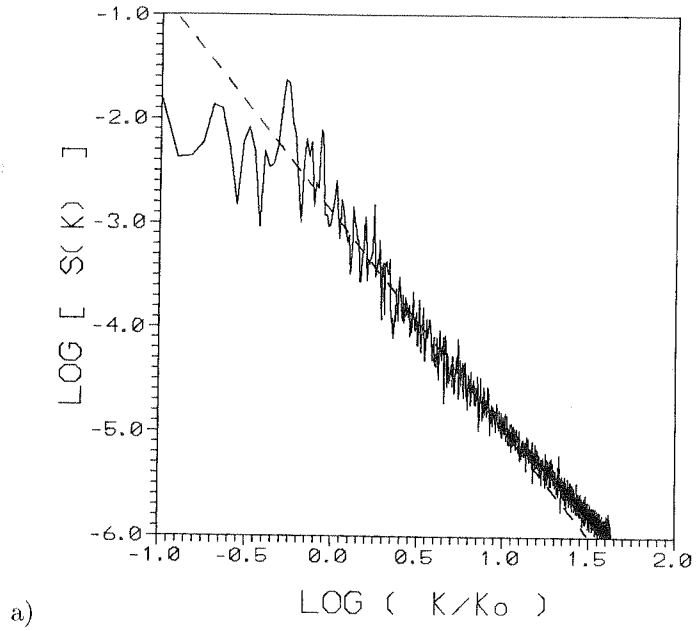

a)

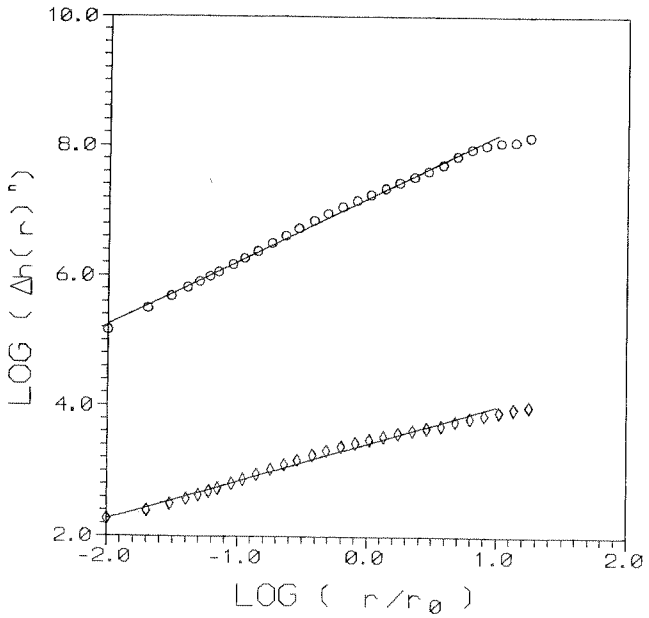

b)

Fig. 14. — a) Spectrum $S(K)$ of $h(x, y)$ as a funtion of K, measured in a sample with $V_f = 680$ m/s. The straight line is a best fit at $K^{-2}(2\pi/K_o = 1$ mm). b) Profile structure functions of order 2 (○) and 1 (◇) as a function of r ($r_o = 1$ mm) measured in a crack with $V_f = 680$ m/s. The straight lines are power law best fits $r^{\zeta(n)}$, with $\zeta(2) \simeq 1$ and $\zeta(1) \simeq 0.6$.

this difference are not clear and are the subject of current investigation. These other materials are heterogeneous materials as different as glass, ceramics, metallic alloys, rocks *etc.*, observed within the domain of heterogeneity, for all sorts of velocities. The origin of the roughness in these cases is more of "microstructural " origin (driven by the disorder) [27–29], while in the experiments described here, the dynamic instability generates the surface roughness. A quantity like $W(r)$ is certainly not sufficient to fully characterized the statistical properties of $h(x, y)$, but higher order moments of the fluctuations of $h(x, y)$ on the scale r should also be studied. This can be done by means of the structure functions

$$\Delta h(r)^n = \langle |h(x + r, y) - h(x, y)|^n \rangle_x \tag{7}$$

If the field $h(x, y)$ has self similar properties the structure functions should scale as a power law that is: $\Delta h(r)^n \propto r^{\zeta(n)}$. This kind of analysis which is usually done in turbulence has been only recently applied to the study of surfaces [22, 25, 26]. In Figure 14b, the structure functions of order 2 and 1 are shown as a function of the distance r for the fastest crack with $V_f = 680$ m/s. We see that the exponent are consistent with those of the spectra and of the rms, because $\zeta(2) = 2\alpha$. The discrepancy of these exponents with those measured in other materials remain an open problem.

8. Conclusions

We have extended the experimental results of references [3, 4] by studying the properties of smooth *versus* rough samples. The novel features of this investigations are:

i) We have characterized the dependence of the steady state velocity and the initial acceleration of a crack on the applied stress. We propose a simple fit of the experimental data which extrapolated to zero velocity roughly predicts the surface energy measured in PMMA in very slow cracks. We have also pointed out in Appendix the importance, for fast cracks, of considering the dependence of the Young modulus on the frequency.

ii) We have checked that the observed properties do not depend on the plate thickness b in the interval $1 < b < 10$ mm.

iii) We have found that the dynamical and statistical properties of the crack are controlled by the steady state velocity as well as the local velocity. We observed the existence of several thresholds for the three properties measured: roughness, sound emission and velocity oscillations. The most pronounced from them is $V_c \simeq 0.5V_R$ where the appearance of the roughness is associated with a strong sound emission and broad band velocity oscillations. However we observe a very weak sound emission associated with velocity oscillations at $V(l) > V_u \simeq (0.32 \pm 0.04)V_R$. The threshold V_u is close to the microbranching transition as suggested in reference [18]. The macrobranching phenomenon, which could be associated to the same crack instability, occurs even at higher values of $V(l)$ at about $V_b \simeq 0.65V_R$. However this last threshold is not reproducible in the sense that we have many samples where V_f was higher than V_b and the crack did not branch. This macrobranch occurs only in the fastest cracks whith $V_f \simeq 0.75V_R$, when a sufficiently large strain is applied to the sample.

iv) We have applied several techniques in order to clarify the properties of the cross correlation among velocity, sound and surface roughness. In Section 6 we have shown that sound is strongly correlated with the velocity oscillations. The existence of this correlation opens a problem on the understanding of the mechanisms producing the roughness

instability above V_c. We have observed that this correlation is present also at $V < V_c$. Therefore one wonder whether it is the increase of sound emission which forces the onset of the roughness or, in contrast, it is the onset of the roughness which could make the sound emission very strong. The recent measurements of Sharon *et al.* [7] show the onset of side microbranching for crack speeds which are close to those where we observe velocity oscillations and weak sound emission. This microbranching, from which the roughness develops, may be at the origin of the weak sound emission observed for $V < V_c$.

v) Finally we have shown that also the statistical properties of the surface are a function of V_f. Specifically we have observed that the scaling exponents characterizing the surface profile are not constant but depend on the crack speed.

All these results have been carefully checked only on PMMA samples. Although we have used different PMMA, whose E varied by a factor of 2, one wonders whether these results are strictly related to PMMA or are general features of brittle materials.

Acknowledgments

We acknowledge useful discussions with J. Fineberg and S. Roux and the technical support by M. Moulin, C. Laroche and D. Bouraya.
This work has been partially supported by DRET contract 92/1446/A000/DRET and CEE contract CHRX-CT-0546.

Appendix

Elastic Constants of PMMA

The value of the Rayleigh wave speed V_R merits a special comment. It is very well-known that in many solids the Young modulus E depends on the frequency at which it is measured, so does the V_R. In the text, in order to compare the results with those of previous works, we have used the same value as in reference [3] which is $V_R = 930$ m/s for $E = 3 \times 10^9$ N/m^2

However this value of V_R does not correspond to the one measured at high frequencies. Let us consider, for example, a PMMA sample whose Young modulus, statically measured with the tensil machine, is $E_o = 3 \times 10^9$ N/m^2, which corresponds to the value given in references [2,3]. In this sample we have then measured the longitudinal waves and transverse waves velocities, called V_L and V_T respectively. This has been done using the time of flights of a burst in a range of frequencies between 0.6 and 1 MHz, which are close to the frequencies detected in the experiment. We find $V_L = 2660$ m/s and $V_T = 1400$ m/s. Using these values one deduces the Poisson coefficient $\sigma = 0.33$, $E' = 6 \times 10^9$ N/m^2 and $V_R = 1300$ m/s. These values are in agreement with those reported in literature [2], obtained with different methods. E' is twice E_o and V_R is 30% larger than the value reported in the text. The latter is obtained, as it has been done in references [3] and [4], using the measured values of E_o and V_L. From this one gets $\sigma = 0.42$, $V_T = 984$ m/s and $V_R = 928$ m/s. This is a reasonable reference value that we used in the text as done in reference [3]. However the dependence of E on the frequency is a very important fact because crack propagation is a fast phenomenon and the value E' has to be taken into account. Therefore the highest value of V_R should be probably the most appropriate. At this point one realizes that the saturation velocity is about $0.6V_R$. This is clearly an open problem which, although known [2], has never been seriously considered in models of crack propagation [1].

References

[1] For a general review see: Freund L.B., Dynamical Fracture Mechanics, (Cambridge Univ. Press, New York, 1990); Kanninen M.F. and Popelar C., Advanced Fracture Mechanics, (Oxford University Press, New York, 1985).
[2] Green A.K. and Pratt L., *Eng. Fract. Mech.* **6** (1974) 71.
[3] Fineberg J., Gross S.P., Marder M. and Swinney H.L., *Phys. Rev. Lett.* **67** (1991) 457; *Phys. Rev. B* **45** (1992) 5146.
[4] Gross S.P., Fineberg J., Marder M., McCormick W.D. and Swinney H.L., *Phys. Rev. Lett.* **71** (1993) 3162.
[5] Marder M. and Gross S.P., *J. Mech. Phys. Solid.* **43** (1995) 1.
[6] Boudet J.F., Steinberg V. and Ciliberto S., *Europhys. Lett.* **30** (1995) 337.
[7] Sharon E., Fineberg J., Gross S.P., *Phys. Rev. Lett.* **74** (1995) 5096.
[8] Abraham F.F., Brodbeck D., Rafey P.A. and Rudge W.E., *Phys. Rev. Lett.* **73** (1994) 272.
[9] Marder M. and Liu X., *Phys. Rev. Lett.* **71** (1993) 2417.
[10] Barber M., Donley J. and Langer J.S., *Phys. Rev. A* **40** (1989) 366.
[11] Langer J.S., *Phys. Rev. A* **46** (1992) 3123.
[12] Langer J.S., *Phys. Rev. Lett.* **70** (1993) 3592.
[13] Ching E., *Phys. Rev. E* **49** (1994) 3382.
[14] Runde K., *Phys. Rev. E* **49** (1994) 2597.
[15] Ching E., Langer J.S. and Nakanishi H., *Phys. Rev. Lett.* **76** (1996) 1087 and preprint (1996).
[16] Lund F., *Phys Rev. Lett.* **76** (1996) 2742.
[17] Arecchi F.T., Bertani D. and Ciliberto S., *Opt. Commun.* **31** (1979) 263.
[18] Sharon E., Gross S.P. and Fineberg J., *Phys. Rev. Lett.* **76** (1996) 2117.
[19] Doll W., *Eng. Fract. Mech.* **5** (1973) 259.
[20] Papoulis A., Probability, Random Variables and Stochastic Process (Mc Graw Hill, 1984).
[21] Monin A.S. and Yaglom A.M., Statistical Fluid Mechanics (MIT Press, Cambridge Massachusetts, 1975).
[22] Schmittbuhl J., Schmitt F. and Scholz C., *J. Geophys. Res.* **100** (1995) 5953.
[23] Schmittbuhl J., Roux S. and Berthaud Y., *Europhys. Lett.* **28** (1995) 585.
[24] Engoy T., Maloy K.J., Hansen A. and Roux S., *Phys. Rev. Lett.* **73** (1994) 834.
[25] Bouchaud J.P., Bouchaud E., Lapasset G. and Planes J., *Phys. Rev. Lett.* **71** (1993) 2240.
[26] Krug J., *Phys Rev. Lett.* **72** (1994) 2907.
[27] Mandelbrot B.B., Passoja D.E. and Paullay A.J., *Nature* **308** (1984) 721.
[28] Bouchaud E., Lapasset G. and Planes J., *Europhys. Lett.* **13** (1990) 73.
[29] Maloy K.J., Hansen A., Hinrichsen E. L. and Roux S., *Phys. Rev. Lett.* **68** (1992) 213.